High Lattice Match Growth of InAsSb Based Materials by Molecular Beam Epitaxy *

Yang Ren(任洋)[1], Rui-Ting Hao(郝瑞亭)[1**], Si-Jia Liu(刘思佳)[1], Jie Guo(郭杰)[1], Guo-Wei Wang(王国伟)[2,3], Ying-Qiang Xu(徐应强)[2,3**], Zhi-Chuan Niu(牛智川)[2,3]

[1]*Key Laboratory of Renewable Energy Advanced Materials and Manufacturing Technology (Ministry of Education), Provincial Key Laboratory of Rural Energy Engineering, Institute of Solar Energy, Yunnan Normal University, Kunming 650092*

[2]*State Key Laboratory for Superlattices and Microstructures, Institute of Semiconductors, Chinese Academy of Sciences, Beijing 100083*

[3]*Synergetic Innovation Center of Quantum Information and Quantum Physics, University of Science and Technology of China, Hefei 230026*

(Received 4 July 2016)

High lattice match growth of InAsSb based materials on GaSb substrates is demonstrated. The present results indicate that a stable substrate temperature and the optimal flux ratios are of critical importance in achieving a homogeneous InAsSb based material composition throughout the growth period. The quality of these epilayers is assessed using a high-resolution x-ray diffraction and atomic force microscope. The mismatch between the GaSb substrate and InAsSb alloy achieves almost zero, and the rms surface roughness of InAsSb alloy achieves around 1.7 Å over an area of 28 μm × 28 μm. At the same time, the mismatches between GaSb and InAs/InAs$_{0.73}$Sb$_{0.27}$ superlattices (SLs) achieve approximately 100 arcsec (75 periods) and zero (300 periods), with the surface rms roughnesses of InAs/InAs$_{0.73}$Sb$_{0.27}$ SLs around 1.8 Å (75 periods) and 2.1 Å (300 periods) over an area of 20 μm×20 μm, respectively. After fabrication and characterization of the devices, the dynamic resistance of the n-barrier-n InAsSb photodetector near zero bias is of the order of 10^6 Ω·cm^2. At 77 K, the positive-intrinsic-negative photodetectors are demonstrated in InAsSb and InAs/InAsSb SL (75 periods) materials, exhibiting fifty-percent cutoff wavelengths of 3.8 μm and 5.1 μm, respectively.

PACS: 81.05.Ea, 81.15.Hi DOI: 10.1088/0256-307X/33/12/128101

Strained-layer superlattices (SLs) have become an increasingly active topic of research since their conception in the 1970s. The InAs/GaSb SL material system has demonstrated a long Auger lifetime, which makes it a promising candidate for improving current HgCdTe (MCT) devices.[1,2] However, devices made from this material system have not shown the expected improvement owing to a comparatively high level of generation-recombination (G-R) dark current. This G-R current arises from a low Shockley–Read–Hall (SRH) carrier lifetime,[3–5] which is currently attributed to native defects in the GaSb layer.[6] A significantly longer minority carrier lifetime has been obtained in the InAs/InAsSb SL system as compared with an InAs/GaSb T2SL operating in the same wavelength range.[7] The increase in minority carrier lifetimes, along with demonstrated bandgap adjustability[8] and suppressed Auger recombination rates,[9] suggest lower dark currents for InAs/InAsSb SL detectors in comparison with their InAs/GaSb T2SL counterparts. The InAs$_{1-x}$Sb$_x$ material has received increasing interest in recent years due to its potential application in the proposed ultra-low loss fiber communication system,[10] which is expected to operate in the 2–4 μm wavelength range. Moreover, in recent years, infrared detectors with multiband detection capabilities are important for highly demanding applications in target identification, recognition, and tracking. Sb-based dual-band detectors have been fabricated and characterized.[11–16] Designing our next experimental study programs, a dual-band detector tailored to detect wavelengths in the range of 1.8–5 μm will be fabricated and characterized. The first band consists of an InAsSb nBn architecture for short wavelength detection, and the second band consists of an InAs/GaSb superlattice pin architecture for medium wavelength detection (nBn: n-barrier-n, which consists of an n-type narrow bandgap thin contact layer and a thick n-type narrow bandgap absorber layer separated by a wide bandgap material layer with a large barrier for electrons and no barrier for holes).

With the InAsSb alloy and the InAs/InAsSb SLs, the lattice mismatch, which increases rapidly with increasing the Sb content, makes the growth of high quality epitaxial layers difficult. Very recently, successful growth of InAsSb lattice matched top (100) GaSb by molecular beam epitaxy (MBE) has been reported.[17]

In this Letter, we describe details of the growth conditions to achieve high lattice match growth of InAsSb based materials on GaSb substrates, including InAsSb ternary compound and InAs/InAsSb heterostructure superlattices. The results of the sur-

*Supported by the National Natural Science Foundation of China under Grant Nos 11474248, 61176127, 61006085, 61274013 and 61306013, the Key Program for International S&T Cooperation Projects of China under Grant No 2011DFA62380, and the Ph.D. Programs Foundation of the Ministry of Education of China under Grant No 20105303120002.

**Corresponding author. Email: ruitinghao@semi.ac.cn; yingqxu@semi.ac.cn

© 2016 Chinese Physical Society and IOP Publishing Ltd

face morphology and crystal structure properties of material characterization of these MBE grown high-quality InAsSb based materials are also presented. The optical and electrical performances of the grown InAsSb based material lattices matched to GaSb are also roughly described.

MBE is a powerful technique for epitaxial growth with excellent crystalline quality and good compositional and doping uniformity. Given the ability to precisely actuate the shutter sequences, MBE has been successfully applied for superlattice growth where the layer thickness needs to be under perfect control. The doping levels can also be controlled with high precision.[18,19]

The material was grown by using a Veeco Gen II molecular beam epitaxy system equipped with valved cracker sources for group V (Sb_2 and As_2) fluxes and Ga/In SUMO® cells, on n-type epiready GaSb (001) substrates. For growing InAsSb lattice-matched to (001) GaSb, a high As_2 flux density ($\sim 3\times10^{-6}$ Torr) was required to stabilize the overall growth, and a small amount of Sb_2 was introduced to fine tune the lattice matching.[20] The incorporation of Sb and As into the epilayer was very sensitive to the stability of substrate temperature and flux ratios.[21] The challenge of the work resides in the control of small antimony flux. Moreover, the day-to-day variation of the Sb flux at the same valve position was greater than the flux needed for the growth. Therefore, relying only on the valve position would make the growth irreproducible.

The photodiode material structures were grown at $T_s = T_c$+70℃ (at Sb cracker temperature is 1000℃), T_c+50℃ (at Sb cracker temperature is 1000℃) or T_c+60℃ (at Sb cracker temperature is 900℃), where T_c is defined as the crossover temperature at which a GaSb surface reconstruction ($2\times5\leftrightarrow1\times3$) at a given antimony stabilization flux, and T_s is defined as the growth temperature or the substrate temperature, according to a calibrated pyrometer.

Adequate removal of the native oxide layer and impurities at the substrate surface prior to epitaxial growth is crucial in production of high-quality optoelectronic devices.[22] Growth temperatures were calibrated by using the above-mentioned reconstructed temperature as a standard. The surface oxide of the GaSb substrate was thermally desorbed at ~630℃ under a vacuum for 15–20 min, and the epilayers have been grown at various temperatures between 510℃ and 560℃ (according to a calibrated pyrometer) with the growth rate of ~0.66 μm/h.

First, a 0.2–0.3 μm nominally undoped GaSb buffer layer was deposited. Then, a 0.6–0.7 μm thick $InAs_{0.91}Sb_{0.09}$ alloy or $InAs/InAs_{0.73}Sb_{0.27}$ SL was grown. Finally, it can be selected to cap with a 50-nm-thick GaSb top contact layer. The V/III beam equivalent pressure ratio was about 10 for As:In, about 0.2 for Sb:In (InAsSb alloy). The cracker tip temperature for As cells was 900℃. The improved material growth was achieved by greatly reduced lattice mismatch between the epilayers and the substrate. The reduced lattice mismatch was achieved by selecting superlattices with less than 0.1% predicted mismatch. This was calculated by comparing the weighted average (θ) of InAsSb based materials and GaSb lattice constants with that of the substrate.[23] The weights were chosen to be the number of layers of each material (75 periods or 300 periods). The III/V ratio for each layer and the growth temperature were optimized by using structural characterization techniques such as AFM and x-ray diffraction.[18]

The surface morphology of the samples is studied with a digital S-II Nano Navi atomic force microscope (AFM). According to previous works, the theoretical studies as well as experimental results show the strong correlation between the surface roughness and the properties of the material. In AFM, a good surface is characterized by long and steady atomic steps, and no mountain-like or valley-like defects. The surface roughness should be on the order of 1.2–1.8 Å over an area of 20 μm × 20 μm, and around 1.0 Å over an area of 5 μm × 5 μm and smaller.[18]

The structural quality of the as-grown material is assessed by high-resolution x-ray diffraction (HRXRD) performed with a Philips x-ray diffractometer using the Cu $K_{\alpha1}$ line. A good HRXRD is recognized by high order diffraction, small mismatch between the epitaxial layers and the substrate, and small full width at half maximum (FWHM) of the diffraction patterns.

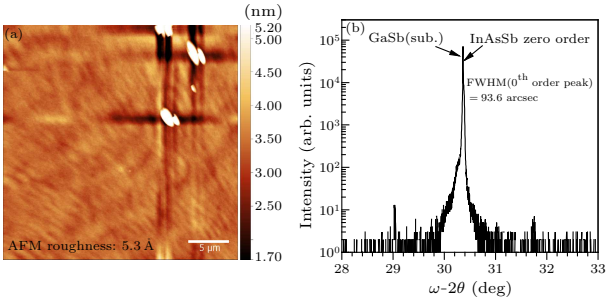

Fig. 1. (a) AFM image of the first InAsSb alloy sample surface over 28 μm × 28 μm. (b) The high-resolution x-ray diffraction of the InAsSb layer. The lattice mismatch between the epitaxial layer and the substrate is almost zero.

We have achieved an rms surface roughness of the first InAsSb alloy material sample (T_c+70℃ (the growth temperature), Sb: 1000℃/580℃ (the cracker tip temperature and base temperature for Sb cells are 1000℃ and 580℃)) around 5.3 Å over an area of 28 μm × 28 μm, the morphology of a typical structure shows bump-like defects. Figure 1(a) shows the surface morphology of a sample.

Figure 1(b) shows the typical x-ray diffraction pattern of the photodiode structures. The As/Sb flux ratio is adjusted until the XRD pattern shows a nearly zero lattice mismatch between the InAsSb layer and the GaSb substrate. The FWHM of the zeroth-order

peak is below 100 arcsec for the device growth. The high lattice match growth of the InAsSb layer has been achieved.

Through the above experimental data, we hypothesize that the poor surface topography may be due to the relatively high growth temperature.[24] By adjusting the growth substrate temperature, we have achieved an rms roughness of the optimized InAsSb alloy material sample (T_c+60℃, Sb: 900℃/580℃) around 1.7 Å over an area of 28 μm × 28 μm. Figure 2 shows the structural characterization results of the InAsSb layer growth. AFM routinely exhibits uniform atomic steps with the rms roughness less than 0.9 Å at 5 μm × 5 μm scan.

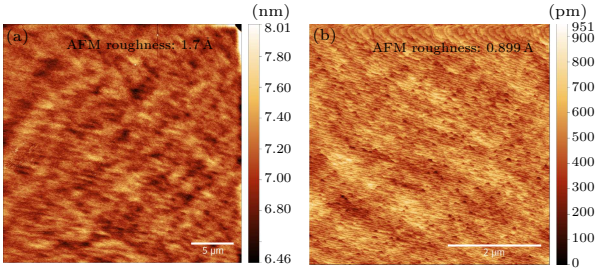

Fig. 2. (a) AFM image of the optimized InAsSb alloy sample surface over 28 μm × 28 μm. (b) AFM image of the optimized InAsSb alloy sample surface over 5 μm × 5 μm.

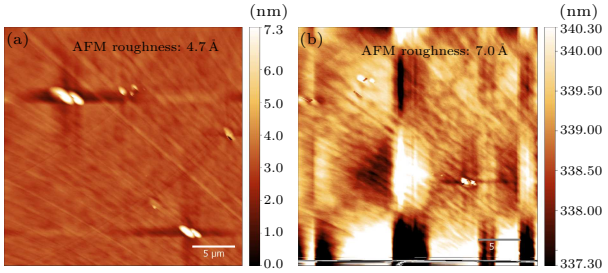

Fig. 3. AFM images of the first long-period thickness InAs/$InAs_{0.73}Sb_{0.27}$ SL sample surface (a) and the first short-period thickness InAs/$InAs_{0.73}Sb_{0.27}$ SL sample surface (b) over 20 μm × 20 μm.

We have achieved the rms roughness of the first long-period thickness (75 periods) InAs/$InAs_{0.73}Sb_{0.27}$ SL sample (T_c+70℃, Sb: 1000℃/580℃) around 4.7 Å over an area of 20 μm × 20 μm and the rms roughness of the first short-period thickness (300 periods) InAs/$InAs_{0.73}Sb_{0.27}$ SL sample (T_c+70℃, Sb: 1000℃/580℃) around 7.0 Å over an area of 20 μm × 20 μm. The sample surfaces have an overall rougher surface morphology with the clear pyramid protrusion and bump-like defects shown in Fig. 3.

By observing the surface morphology of the experimental samples, we speculate that the relatively high growth temperature has a certain influence. At the same time, analyzing the XRD chart, these defects appear to be Sb-deficient, whereas the As and In contents remain constant. On the other hand, too low a Sb_2 flux density usually results in poor surface morphology as shown in Fig. 3, and there is the broad FWHM of the zeroth-order peak even under close lattice-matched conditions as shown in Fig. 4.

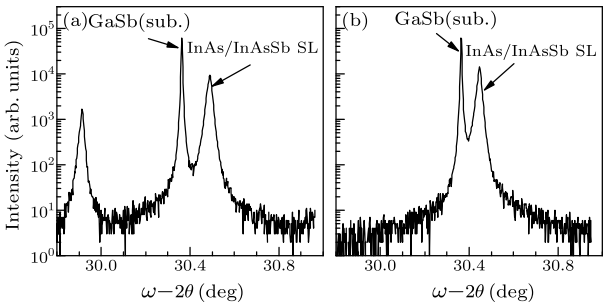

Fig. 4. High-resolution x-ray diffraction of the first InAs/InAsSb SLs. (a) The long-period thickness (75 periods) InAs/$InAs_{0.73}Sb_{0.27}$ SL, and (b) the short-period thickness (300 periods) InAs/$InAs_{0.73}Sb_{0.27}$ SL.

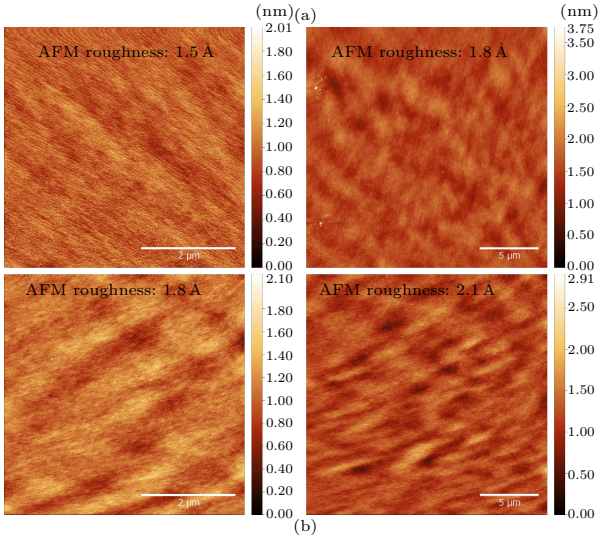

Fig. 5. AFM images of the optimized long-period thickness (75 periods) InAs/$InAs_{0.73}Sb_{0.27}$ SL sample surface (a) and the optimized short-period thickness (300 periods) InAs/$InAs_{0.73}Sb_{0.27}$ SL sample surface (b) over 20 μm × 20 μm and 5 μm × 5 μm.

To optimize growth of the superlattice material, we adjusted the growth substrate temperature and the Sb_2 flux density, after that, we achieved the rms roughness of the optimized long-period thickness (75 periods) InAs/$InAs_{0.73}Sb_{0.27}$ SL sample and the optimized short-period thickness (300 periods) InAs/$InAs_{0.73}Sb_{0.27}$ SL sample (T_c+60℃, Sb: 900℃/580℃) separately around 1.8 Å and 2.1 Å over an area of 20 μm × 20 μm. By carefully adjusting the flux stability, growth temperature and shutter movements, we have been able to grow InAs/$InAs_{0.73}Sb_{0.27}$ SLs with very smooth surfaces. In Fig. 5, in a 5 μm × 5 μm scan (right), very clear atomic steps and smooth defect-free surface are observed, and long atomic steps with rms roughnesses of 1.5 Å and 1.8 Å are obtained. In addition, in the larger surface scan (20 μm × 20 μm), no growth defects is visible.

The mismatch between the zeroth-order peak of the optimized long-period thickness (75 peri-

ods) InAs/$InAs_{0.73}Sb_{0.27}$ SL and the GaSb substrate peak is approximately 100 arcsec, while the FWHM of the zeroth-order peak is below 130 arcsec for the grown devices. The lattice mismatch between the optimized short-period thickness (300 periods) InAs/$InAs_{0.73}Sb_{0.27}$ SL and the GaSb substrate is almost zero. The symmetric and narrow widths of the superlattice fundamental x-ray diffraction peak as shown in Fig. 6 indicate that very close lattice matching is achieved. The Sb concentration is adjusted for close lattice matching to GaSb.

The SL-period thickness and the lattice mismatch between the SL and the GaSb substrate are determined from the HRXRD measurements.[25] As shown in Fig. 6(a), x-ray diffraction exhibits high order satellite peaks. In spite of the thin structure (0.6–0.7 μm), the satellite peaks appear up to the third order with a measured period of 93.3 Å (theoretical value is 87.7 Å). The measured period of the short-period thickness (300 periods) InAs/$InAs_{0.73}Sb_{0.27}$ SL is about 24.6 Å (theoretical value is 21.9 Å) as shown in Fig. 6(b). There is a certain deviation between theoretical values and experimental values. The change of SL-period thickness does not affect the composition of superlattice components, theoretically. So, we calibrate the speed of In during the next growth process using the calculated thickness.

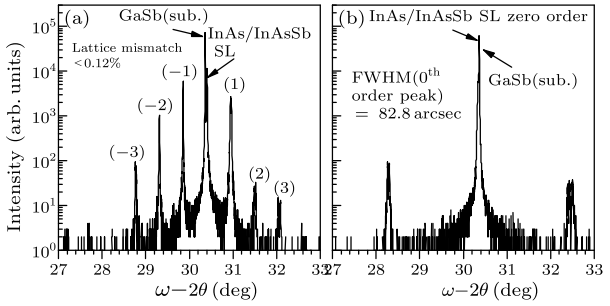

Fig. 6. (a) High-resolution x-ray diffraction of the optimized long-period thickness (75 periods) InAs/$InAs_{0.73}Sb_{0.27}$ SL. (b) High-resolution x-ray diffraction of the optimized short-period thickness (300 periods) InAs/$InAs_{0.73}Sb_{0.27}$ SL.

When the cracker tip temperature and base temperature for Sb cells are 900℃ and 580℃, respectively, T_c+60℃ (T_c+50℃ (corresponding to the cracker tip temperature for Sb cells is 1000℃)) is the optimum growth temperature for InAsSb alloy or InAs/$InAs_{0.73}Sb_{0.27}$ SL.

Prior to detector growth, the InAs/InAsSb SL growth conditions are optimized with respect to the substrate temperature and As/Sb beam equivalent pressure (BEP) ratio.[18,24,26] The results of this optimization process show that a substrate temperature of T_c+60℃ with an As/Sb BEP ratio of ∼8 (the long-period thickness (75 periods) InAs/$InAs_{0.73}Sb_{0.27}$ SL) or ∼9 (the short-period thickness (300 periods) InAs/$InAs_{0.73}Sb_{0.27}$ SL) results in the high lattice match growth of the InAs/$InAs_{0.73}Sb_{0.27}$ SL material.

Photodetectors are fabricated by using an ICP dry etch and a standard photolithographic process. Ti/Pt/Au metallization is evaporated in a liftoff process to form ohmic contacts. The devices fabricated into single-pixel mesa structures are completed without any anti-reflecting coating and surface passivation. Figure 7 shows the results of the electrical and optical characteristics of InAsSb based material photodetectors. Measurements of nBn dark currents as a function of bias are shown in Fig. 7(a). Figure 7(a) (inset) shows the nBn device and R_0A versus V relation of the device. Analyzing the measured dark current density-voltage (J–V) and dynamic resistance-area versus bias voltage (R_0A–V) characteristics of the InAsSb nBn photodetector are presented. A measured dark current density of 7.525×10^{-5} mA/cm^2 under a bias of −0.1 V over a mesa size of 200 μm × 200 μm, and a maximum differential-resistance-area-product of 4×10^6 Ω·cm^2 near zero bias (very small bias) are achieved, at 77 K. The InAsSb positive-intrinsic-negative (PIN) device exhibits photoresponse up to 4 μm at 77 K. The 50% cutoff wavelength of the spectral response curve is 3.8 μm, which is in the MWIR regime. The QE of the InAsSb PIN device is measured by taking photocurrent measurements with a calibrated blackbody source at 800℃. At 77 K, a peak responsivity of 0.474 A/W is obtained at the wavelength of 2.78 μm, which represents a peak quantum efficiency of 21.4%.

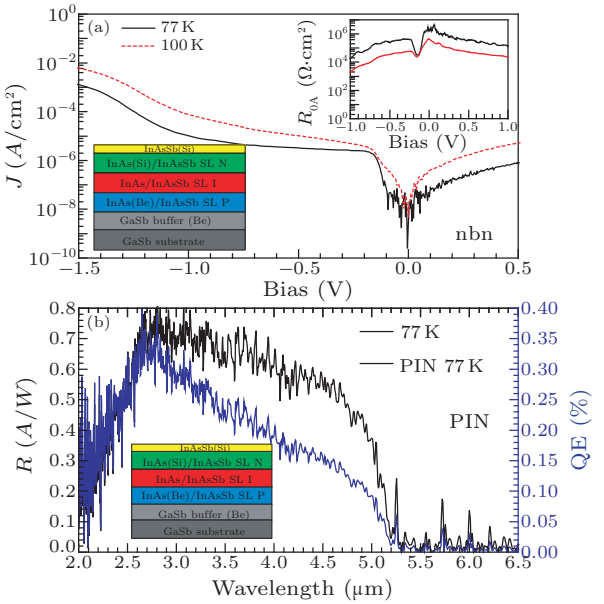

Fig. 7. (a) Dark current density as a function of the applied bias of the InAsSb nBn photodetector at 77 K and 100 K. Inset: schematic diagram of an nBn device and R_0A versus V relation of the device. (b) Front side illuminates single pass spectral responsivity spectrum and quantum efficiency spectrum for the photodetector under zero bias, measured at 77 K. Inset: schematic diagram of a PIN InAs/InAsSb SL device.

Mid-wave infrared Ga-free InAs/$InAs_{0.73}Sb_{0.27}$ (75 periods) type-Ⅱ superlattice (T2SL) PIN photodetectors have been fabricated on GaSb substrates. The spectral photoresponse curve and quantum efficiency

spectrum at 77 K are presented in Fig. 7(b). The measurements are carried out under zero bias with the photodiodes illuminated from the front side at normal incidence. The resulting mid-infrared photovoltaic detectors measured at 77 K exhibit a 50% cutoff wavelength of 5.1 μm, and a peak responsivity of 0.883 A/W over a mesa size of 50 μm × 50 μm. Peak quantum efficiency (QE) of 34.6% at 2.78 μm over a mesa size of 50 μm × 50 μm is achieved.

In summary, we have shown that stable substrate temperature and optimal control on the flux ratios are of critical importance to grow high-quality InAsSb alloy and InAs/InAsSb superlattice lattice matched to GaSb. Narrow FWHM of InAsSb indicates that homogeneous composition along the growth direction is achieved, and the epilayer crystallinity is substrate limited. From the AFM and the HRXRD measurement structure of the materials, the high lattice match growth of InAsSb based materials have been demonstrated. After the adjustment and optimization of the sample materials, we have achieved the requirements to fabricate devices and studied the optical properties and electrical characteristics of the device material. Structure based on nBn design of the InAsSb photodetector shows the dark current density of 7.525×10^{-5} mA/cm^2 ($V_b = -0.1$ V) and the maximum RA product of 4×10^6 Ω·cm^2 ($V_b \approx 0$ V), at 77 K. The corresponding values of 50% cutoff wavelength and quantum efficiency are 3.8 μm and 21.4% (the PIN InAsSb device). Single PIN InAs/InAsSb SL (75 periods) photodiode typical responsivity of 0.883 A/W and 50% cutoff wavelength of 5.1 μm are obtained, at 77 K. The processed device exhibits a quantum efficiency around 34.6%. The optical and electrical characterizations of the MBE grown InAsSb based material lattices matched to GaSb are promising for multiband infrared detectors and infrared portable photodetector applications.

References

[1] Grein C H, Young P M and Ehrenreich H 1992 *Appl. Phys. Lett.* **61** 2905
[2] Youngdale E R, Meyer J R, Hoffman C A, Bartoli F J, Grein C H, Young P M, Ehrenreich H, Miles R H and Chow D H 1994 *Appl. Phys. Lett.* **64** 3160
[3] Grein C H, Garland J and Flatte M E 2009 *J. Electron. Mater.* **38** 1800
[4] Rhiger D R 2011 *J. Electron. Mater.* **40** 1815
[5] Donetsky D, Svensson S P, Vorobjev L E and Belenky G 2009 *Appl. Phys. Lett.* **95** 212104
[6] Svensson S P, Donetsky D, Wang D, Hier H, Crowne F J and Belenky G 2011 *J. Cryst. Growth* **334** 103
[7] Steenbergen E H, Connelly B C, Metcalfe G D, Shen H, Wraback M, Lubyshev D, Qiu Y, Fastenau J M, Liu A W K, Elhamri S, Cellek O O and Zhang H Y 2011 *Appl. Phys. Lett.* **99** 251110
[8] Lackner D, Steger M, Thewalt M L W, Pitts O J, Cherng Y T, Watkins S P, Plis E and Krishna S 2012 *J. Appl. Phys.* **111** 034507
[9] Ciesla C M, Murdin B N, Pidgeon C R, Stradling R A, Phillips C C, Livingstone M, Galbraith I, Jaroszynski D A, Langerak C J G M, Tang P J P and Pullin M J 1996 *J. Appl. Phys.* **80** 2994
[10] Tran D, Sigel Jr G H and Bendow B 1984 *J. Lightwave Technol.* **2** 566
[11] Schneider H, Maier T, Fleissner J, Walther M, Koidl P, Weimann G, Cabanski W, Finck M, Menger P, Rode W and Ziegler J 2005 *Infrared Phys. Technol.* **47** 53
[12] Rogalski A 2011 *Infrared Phys. Technol.* **54** 136
[13] Gautam N, Naydenkov M, Myers S, Barve A V, Plis E, Rotter T, Dawson L R and Krishna S 2011 *Appl. Phys. Lett.* **98** 121106
[14] Khoshakhlagh A, Rodriguez J B, Plis E, Bishop G D, Sharma Y D, Kim H S, Dawson L R and Krishna S 2007 *Appl. Phys. Lett.* **91** 263504
[15] Plis E, Naydenkov M, Myers S, Klein B, Gautam N, Krishna S S, Smith E P, Johnson S and Krishna S 2013 *Infrared Phys. Technol.* **59** 28
[16] Refaat T F, Abedin M N, Bhat I B and Xiao Y 2005 *Opt. Eng.* **44** 120501
[17] Tsang W T, Chiu T H, Kisker D W and Ditzenberger J A 1985 *Appl. Phys. Lett.* **46** 283
[18] Nguyen B M 2010 *Dissertation Abstracts Int.* **72-02** 391
[19] Mohammedy F M and Deen M J 2009 *J. Mater. Sci.: Mater. Electron.* **20** 1039
[20] Chang C A, Ludeke R, Chang L L and Esaki L 1977 *Appl. Phys. Lett.* **31** 759
[21] Lee G S, Lo Y, Lin Y F, Bedair S M and Laidig W D 1985 *Appl. Phys. Lett.* **47** 1219
[22] Neuberger M 1971 *Handbook of Electronic Materials: 3-5 Semiconducting Compounds* (New York: IFI/Plenum Data Co.)
[23] Wei Y, Gin A, Razeghi M and Brown G J 2002 *Appl. Phys. Lett.* **80** 3262
[24] Chiu T H, Tsang W T, Ditzenberger J A, Chu S N G and Van der Ziel J P 1986 *J. Appl. Phys.* **60** 205
[25] Rodriguez J B, Christol P, Cerutti L, Chevrier F and Joullié A 2005 *J. Cryst. Growth* **274** 6
[26] Schuler-Sandy T, Myers S, Klein B, Gautam N, Ahirwar P, Tian Z B, Rotter T, Balakrishnan G, Plis E and Krishna S 2012 *Appl. Phys. Lett.* **101** 071111